mathematics

MDPI

Article

Design of Dies of Minimum Length Using the Ideal Flow Theory for Pressure-Dependent Materials

Sergei Alexandrov [1,2] and Vyacheslav Mokryakov [1,*]

[1] Ishlinsky Institute for Problems in Mechanics RAS, 101-1 Prospect Vernadskogo, Moscow 119526, Russia; sergei_alexandrov@spartak.ru
[2] Department of Civil Engineering, RUDN University, 6 Miklukho-Maklaya St., Moscow 117198, Russia
* Correspondence: mokr@ipmnet.ru; Tel.: +7-905-530-82-33

Abstract: This paper develops the ideal plastic flow theory for the stationary planar flow of pressure-dependent materials. Two rigid plastic material models are considered. One of these models is the double-shearing model, and the other is the double slip and rotation model. Both are based on the Mohr–Coulomb yield criterion. It is shown that the general ideal plastic flow theory is only possible for the double slip and rotation model if the intrinsic spin vanishes. The theory applies to calculating the shape of optimal extrusion and drawing dies of minimum length. The latter condition requires a singular characteristic field. The solution is facilitated using the extended R–S method, commonly employed in the classical plasticity of pressure-independent materials. In particular, Riemann's method is used in a region where all characteristics are curved. It is advantageous since determining the optimal shape does not require the characteristic field inside the region. The solution is semi-analytical. A numerical procedure is only required to evaluate ordinary integrals. It is shown that the optimal shape depends on the angle of internal friction involved in the yield criterion.

Keywords: ideal flow; double-shearing model; double slip and rotation model; ideal die shape; extrusion; drawing

MSC: 74C05

check for updates

Citation: Alexandrov, S.; Mokryakov, V. Design of Dies of Minimum Length Using the Ideal Flow Theory for Pressure-Dependent Materials. *Mathematics* **2023**, *11*, 3726. https://doi.org/10.3390/math11173726

Academic Editors: Andrey Jivkov and Paolo Mercorelli

Received: 12 July 2023
Revised: 7 August 2023
Accepted: 28 August 2023
Published: 30 August 2023

Correction Statement: This article has been republished with a minor change. The change does not affect the scientific content of the article and further details are available within the backmatter of the website version of this article.

Copyright: © 2023 by the authors. Licensee MDPI, Basel, Switzerland. This article is an open access article distributed under the terms and conditions of the Creative Commons Attribution (CC BY) license (https://creativecommons.org/licenses/by/4.0/).

1. Introduction

The ideal flow theory is a tool for metal forming design [1]. Considering bulk ideal flows, almost all available results are restricted to rigid perfectly plastic solids obeying Tresca's yield criterion [2,3]. An important feature of this material model is that the complete system of equations is hyperbolic. Therefore, the method of characteristics has been widely adopted for calculating ideal flows. In particular, the pioneering ideal flow solution was provided in [4]. That solution calculates the die profile for maximum strip drawing and extrusion efficiency. The approach developed for constructing the solution consists of matching the characteristic field from the solution for material flow through an infinite wedge-shaped channel with no friction and two characteristic fields in which the characteristics of one family are straight. A general plane strain ideal flow solution for the flow having an axis of symmetry between two surfaces was outlined in [5]. The axisymmetric die profile for maximum drawing and extrusion efficiency was calculated in [6]. This paper introduces an additional criterion of optimality that the die must be of minimum length. The characteristic field must be singular to satisfy this criterion.

The plane strain ideal flow theory was extended to the stationary flow of orthotropic materials in [7], assuming that the evolution of the yield criterion obeys the law proposed in [8]. The solution [4] was generalized for orthotropic materials in [9]. However, the anisotropic properties do not affect the die's shape. This feature is valid for all solutions based on the theory [7]. Therefore, the available plane strain solutions for isotropic materials immediately apply to anisotropic materials. The difference is revealed in calculating stress

fields. It was shown in [10] that stationary axisymmetric ideal flows of anisotropic materials exist if the yield criterion proposed in [11] is adopted.

Many materials obey pressure-dependent yield criteria. Examples of such materials are soils [12,13], metals [14–16], and granular materials [13,17]. Several plasticity models are available for pressure-dependent materials [18,19]. The present paper focuses on the double-shearing model proposed in [20] and the double slip and rotation model proposed in [21]. It is assumed that both are based on the Mohr–Coulomb yield criterion. The method developed in [4] was used in [22] to calculate an ideal flow die for such materials. The general ideal flow theory was not required for that calculation. In particular, the solution for the flow through an infinite wedge-shaped channel with no friction can be easily found. Constructing two regions in which the characteristics of one family are straight is then straightforward. The solution [22] shows that the optimal shapes of dies depend on the angle of internal friction involved in the Mohr–Coulomb yield criterion. Therefore, developing the general ideal flow theory for pressure-dependent materials is desirable.

The present paper develops the ideal flow theory for the stationary planar flow of pressure-dependent materials obeying the models proposed in [20,21]. The constitutive equations of each model reduce to classical metal plasticity at specific values of input parameters. However, it is shown that the general ideal flow theory is possible only in a special case of the double slip and rotation model. Notably, the double slip and rotation model also retains all features inherent to classical plasticity under quite different conditions, resulting in singular velocity fields near certain surfaces, whereas the double-shearing model does not [23].

2. Constitutive Equations

The present paper considers two rigid plastic models of pressure-dependent materials under plane strain deformation. One of these models is the double-shearing model [20], and the other is a special case of the double slip and rotation model [21]. The present section briefly describes these models, as necessary for the subsequent solution. Flow is stationary, and body forces are neglected.

In planes of flow, the principal line coordinate system (ξ, η) is defined by the condition that its coordinate curves coincide with principal stress trajectories. It is evident that this coordinate system is orthogonal. The principal stresses are denoted as σ_ξ and σ_η. It is assumed without loss of generality that

$$\sigma_\xi > \sigma_\eta. \tag{1}$$

The stress equations of both models include the stress equilibrium equations and a yield criterion. The models can be used in conjunction with any yield criterion. However, the Mohr–Coulomb yield criterion is most widely used in the mechanics of granular materials [13,17]. Moreover, only this criterion is compatible with the ideal flow conditions described in the following section. The Mohr–Coulomb yield criterion can be represented as

$$\left(\sigma_\xi + \sigma_\eta\right) \sin\varphi + \sigma_\xi - \sigma_\eta = 2k\cos\varphi, \tag{2}$$

where k is the cohesion and φ is the angle of internal friction. Both are constitutive parameters. The system of stress equations is hyperbolic [20]. The characteristic coordinates are denoted as (α, β). The characteristic directions are symmetric relative to the principal stress directions. In particular,

$$\frac{H_\xi}{H_\eta}\frac{d\xi}{d\eta} = -\tan\left(\frac{\pi}{4} - \frac{\varphi}{2}\right) \quad \text{and} \quad \frac{H_\xi}{H_\eta}\frac{d\xi}{d\eta} = \tan\left(\frac{\pi}{4} - \frac{\varphi}{2}\right). \tag{3}$$

for the α- and β-lines, respectively. Here, H_ξ and H_η are the scale factors of the ξ- and η-coordinate curves, respectively. The characteristic relations are

$$\begin{array}{c} \cos\varphi dp + 2(p\sin\varphi + \cos\varphi)d\psi = 0 \quad \text{along} \quad \text{an } \alpha\text{-line}, \\ \cos\varphi dp - 2(p\sin\varphi + \cos\varphi)d\psi = 0 \quad \text{along} \quad \text{a } \beta\text{-line}. \end{array} \tag{4}$$

Here, ψ is the anticlockwise angular rotation of the ξ-line from any fixed direction in planes of flow. Moreover,

$$p = -\frac{\sigma_\xi + \sigma_\eta}{2k}. \tag{5}$$

Note that the characteristic relations provided in [20] involve the orientation of the α-line instead of ψ. However, it is immaterial because the angle between the α- and ξ-directions is constant, as following from (3).

The velocity equations of the double-shearing model were provided in [20]. If $\partial/\partial s_\alpha$ and $\partial/\partial s_\beta$ denote differentiation along the α- and β-lines, respectively, the velocity relations along the stress characteristics may be written as

$$\cos\varphi\frac{\partial u_\alpha}{\partial s_\alpha} - u_\beta\left(\frac{\partial\psi}{\partial s_\alpha} + \sin\varphi\frac{\partial\psi}{\partial s_\beta}\right) = 0 \text{ and } \cos\varphi\frac{\partial u_\beta}{\partial s_\beta} + u_\alpha\left(\frac{\partial\psi}{\partial s_\beta} + \sin\varphi\frac{\partial\psi}{\partial s_\alpha}\right) = 0. \tag{6}$$

It has been taken into account here that the process is stationary. The velocity equations of the double slip and rotation model were provided in [21]. These equations involve the intrinsic spin. Several physical interpretations of this quantity are possible [24]. It is reasonable in many cases to assume that the intrinsic spin vanishes [25,26]. The present paper is concerned with this special case of the double slip and rotation model. Then, the velocity relations along the stress characteristics may be written as

$$\cos\varphi\frac{\partial u_\alpha}{\partial s_\alpha} + (u_\alpha\sin\varphi - u_\beta)\frac{\partial\psi}{\partial s_\alpha} = 0 \text{ and } \cos\varphi\frac{\partial u_\beta}{\partial s_\beta} + (u_\alpha - u_\beta\sin\varphi)\frac{\partial\psi}{\partial s_\beta} = 0. \tag{7}$$

It is seen that, in contrast to (6), these equations are the velocity characteristic relations.

3. Ideal Flows

The ideal flow condition is that the velocity vector **V** is everywhere tangent to one of the principal stress trajectories.

3.1. The Double Slip and Rotation Model

3.1.1. Characteristic Lines of Both Families Are Curved

Let the velocity vector be tangent to the ξ-lines. Figure 1 illustrates the ideal flow condition and the characteristic coordinate system. In this figure, $\mathbf{e_\xi}$, $\mathbf{e_\alpha}$, and $\mathbf{e_\beta}$ are the unit vectors directed along ξ-, α-, and β-lines, respectively. In the case under consideration, Equations (4) and (7) can be rewritten as

$$\begin{array}{cc} \cos\varphi\frac{\partial p}{\partial\alpha} + 2(p\sin\varphi + \cos\varphi)\frac{\partial\psi}{\partial\alpha} = 0, & \cos\varphi\frac{\partial p}{\partial\beta} - 2(p\sin\varphi + \cos\varphi)\frac{\partial\psi}{\partial\beta} = 0, \\ \cos\varphi\frac{\partial u_\alpha}{\partial\alpha} + (u_\alpha\sin\varphi - u_\beta)\frac{\partial\psi}{\partial\alpha} = 0, & \cos\varphi\frac{\partial u_\beta}{\partial\beta} + (u_\alpha - u_\beta\sin\varphi)\frac{\partial\psi}{\partial\beta} = 0. \end{array} \tag{8}$$

It was shown in [27] that the parametrization of the characteristic lines can be chosen such that

$$\psi = (\alpha + \beta)\cos\varphi. \tag{9}$$

Substituting (9) into (8) yields

$$\begin{array}{cc} \frac{\partial p}{\partial\alpha} + 2(p\sin\varphi + \cos\varphi) = 0, & \frac{\partial p}{\partial\beta} - 2(p\sin\varphi + \cos\varphi) = 0, \\ \frac{\partial u_\alpha}{\partial\alpha} + u_\alpha\sin\varphi - u_\beta = 0, & \frac{\partial u_\beta}{\partial\beta} + u_\alpha - u_\beta\sin\varphi = 0. \end{array} \tag{10}$$

It follows from the geometry of Figure 1 that

$$\mathbf{V} = V\mathbf{e}_{\boldsymbol{\xi}} = u_\alpha \mathbf{e}_{\boldsymbol{\alpha}} + u_\beta \mathbf{e}_{\boldsymbol{\beta}}. \tag{11}$$

Since $\mathbf{e}_{\boldsymbol{\xi}} \cdot \mathbf{e}_{\boldsymbol{\alpha}} = \cos(\pi/4 + \varphi/2)$, $\mathbf{e}_{\boldsymbol{\xi}} \cdot \mathbf{e}_{\boldsymbol{\beta}} = \cos(\pi/4 + \varphi/2)$, and $\mathbf{e}_{\boldsymbol{\beta}} \cdot \mathbf{e}_{\boldsymbol{\alpha}} = -\sin\varphi$, Equation (11) results in

$$u_\alpha = u_\beta = V\frac{\cos(\pi/4 + \varphi/2)}{1 - \sin\varphi}. \tag{12}$$

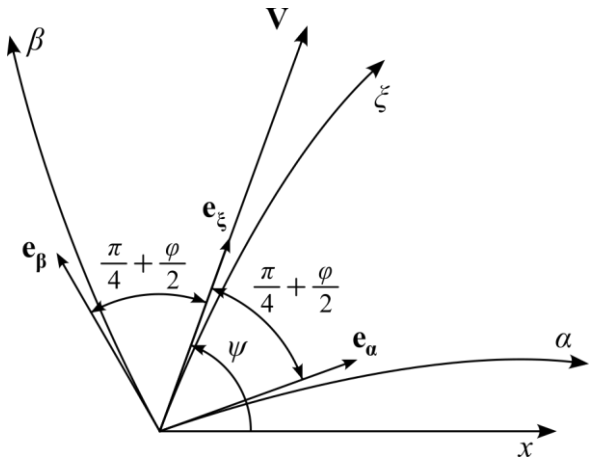

Figure 1. Characteristic lines; the velocity vector is directed along the ξ-lines.

Eliminating u_α and u_β in the last two equations in (10) using (12), one gets

$$\frac{\partial \ln V}{\partial \alpha} = 1 - \sin\varphi \text{ and } \frac{\partial \ln V}{\partial \beta} = -(1 - \sin\varphi). \tag{13}$$

The first two equations in (10) can be integrated to give

$$\ln\left(\frac{p\sin\varphi + \cos\varphi}{p_0\sin\varphi + \cos\varphi}\right) = 2(\beta - \alpha)\sin\varphi, \tag{14}$$

where p_0 is constant. The equations in (13) can also be integrated to give

$$\ln\frac{V}{V_0} = (1 - \sin\varphi)(\alpha - \beta), \tag{15}$$

where V_0 is constant. Equations (14) and (15) are compatible if

$$\frac{V}{V_0} = \left(\frac{p\sin\varphi + \cos\varphi}{p_0\sin\varphi + \cos\varphi}\right)^t, \tag{16}$$

where $t = (\sin\varphi - 1)/(2\sin\varphi)$. Note that

$$\lim_{\varphi\to 0}\left(\frac{p\sin\varphi + \cos\varphi}{p_0\sin\varphi + \cos\varphi}\right)^t = \exp\left(\frac{p_0 - p}{2}\right). \tag{17}$$

Equations (16) and (17) combine to yield

$$\frac{V}{V_0} = \exp\left(\frac{p_0 - p}{2}\right). \tag{18}$$

for pressure-independent materials. This equation coincides with the relation between V and p derived in [4].

Equation (16) ensures the existence of ideal flows. Calculating ideal flows reduces to determining characteristic nets. In particular, Equation (14) provides the distribution of p through a found characteristic net. Then, Equation (16) allows for the magnitude of the velocity vector to be calculated. The direction of this vector is determined as shown in Figure 1. The principal stresses are given by Equations (2) and (5).

Let the velocity vector be tangent to the η-lines (Figure 2). In this case,

$$\mathbf{V} = V\mathbf{e_\eta} = u_\alpha \mathbf{e_\alpha} + u_\beta \mathbf{e_\beta}. \tag{19}$$

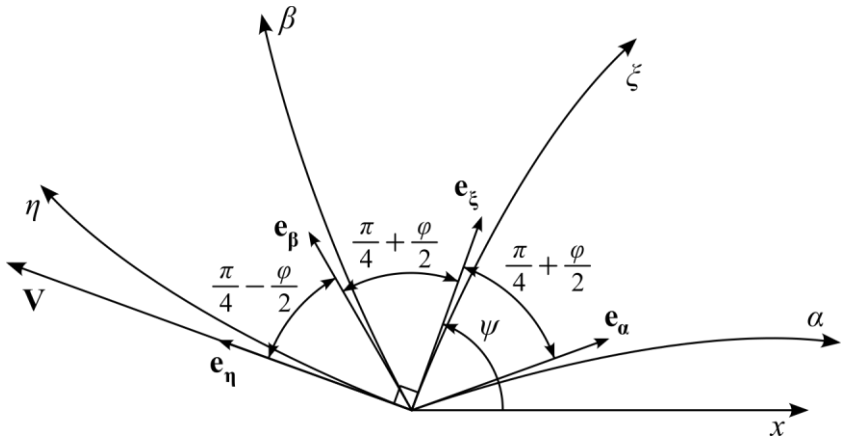

Figure 2. Characteristic lines; the velocity vector directed along the η-lines.

Because $\mathbf{e_\eta} \cdot \mathbf{e_\alpha} = -\cos(\pi/4 - \varphi/2)$, $\mathbf{e_\eta} \cdot \mathbf{e_\beta} = \cos(\pi/4 - \varphi/2)$, and $\mathbf{e_\beta} \cdot \mathbf{e_\alpha} = -\sin\varphi$, Equation (19) results in

$$u_\beta = -u_\alpha = V\frac{\cos(\pi/4 - \varphi/2)}{1 + \sin\varphi}. \tag{20}$$

Similarly to (13), one can get from (10) and (20) that

$$\frac{\partial \ln V}{\partial \alpha} = -(1 + \sin\varphi) \text{ and } \frac{\partial \ln V}{\partial \beta} = 1 + \sin\varphi. \tag{21}$$

Integrating these equations yields

$$\ln\frac{V}{V_0} = (1 + \sin\varphi)(\beta - \alpha), \tag{22}$$

where V_0 is constant. Equations (14) and (22) combine to give

$$\frac{V}{V_0} = \left(\frac{p\sin\varphi + \cos\varphi}{p_0\sin\varphi + \cos\varphi}\right)^{1-t}. \tag{23}$$

This equation connects p and V in ideal flows. Note that

$$\lim_{\varphi\to 0}\left(\frac{p\sin\varphi + \cos\varphi}{p_0\sin\varphi + \cos\varphi}\right)^{1-t} = \exp\left(\frac{p - p_0}{2}\right). \tag{24}$$

Equations (23) and (24) are combined to yield

$$\frac{V}{V_0} = \exp\left(\frac{p - p_0}{2}\right). \tag{25}$$

As in the previous case, calculating ideal flows reduces to determining characteristic nets.

3.1.2. Characteristic Lines of One of the Families Are Straight

Let α-lines be straight and the velocity vector be tangent to the ξ-lines. The angle between any α-line and the x-axis is $\psi - \pi/4 - \varphi/2$ (Figures 1 and 2). This angle is independent of α because the α-line is straight. Therefore, the angle ψ is also independent of α. It follows from the first equation in (4) that p is also independent of α. The second equation in (4) becomes

$$\cos\varphi\frac{dp}{d\beta} - 2(p\sin\varphi + \cos\varphi)\frac{d\psi}{d\beta} = 0. \tag{26}$$

This equation can be immediately integrated to give

$$\ln\left(\frac{p\sin\varphi + \cos\varphi}{p_0\sin\varphi + \cos\varphi}\right) = 2\tan\varphi(\psi - \psi_0), \tag{27}$$

where p_0 and ψ_0 are constant. Equation (9) can be transformed to

$$\psi = (\alpha_0 + \beta)\cos\varphi, \tag{28}$$

where α_0 is constant. Equation (12) is valid. The first equation in (7) and (28) show that u_α is independent of α. Therefore, V and u_β are also independent of α.

Using (12) and (28), one can rewrite the second equation in (13) as

$$\cos\varphi\frac{dV}{d\beta} + V(1 - \sin\varphi)\frac{d\psi}{d\beta} = 0. \tag{29}$$

This equation can be immediately integrated to give

$$\ln\frac{V}{V_0} = -\frac{(1 - \sin\varphi)}{\cos\varphi}(\psi - \psi_0). \tag{30}$$

Equations (27) and (30) are compatible if (16) is satisfied.

Let α-lines be straight and the velocity vector be tangent to the η-lines. As in the previous case, u_α, u_β, and V are independent of α. Equations (20) and (28) are valid. Then, the second equation in (21) can be rewritten as

$$\cos\varphi\frac{dV}{d\beta} - V(1 + \sin\varphi)\frac{d\psi}{d\beta} = 0. \tag{31}$$

Integrating this equation, one gets

$$\ln\frac{V}{V_0} = \frac{(1 + \sin\varphi)}{\cos\varphi}(\psi - \psi_0). \tag{32}$$

Equations (27) and (32) are compatible if (23) is satisfied.

Let β-lines be straight and the velocity vector be tangent to the ξ-lines. Then, the angle ψ is independent of β. It follows from the second equation in (4) that p is also independent of β. The first equation in (4) becomes

$$\cos\varphi\frac{dp}{d\alpha} + 2(p\sin\varphi + \cos\varphi)\frac{d\psi}{d\alpha} = 0. \tag{33}$$

Integrating this equation, one gets

$$\ln\left(\frac{p\sin\varphi + \cos\varphi}{p_0\sin\varphi + \cos\varphi}\right) = -2\tan\varphi(\psi - \psi_0). \tag{34}$$

Equation (9) can be transformed to

$$\psi = (\alpha + \beta_0)\cos\varphi, \tag{35}$$

where β_0 is constant. Equation (12) is valid. The second equation in (7) and (35) show that u_β is independent of β. Therefore, u_α and V are also independent of β. Using (12) and (35), one can rewrite the first equation in (13) as

$$\cos\varphi\frac{dV}{d\alpha} - V(1-\sin\varphi)\frac{d\psi}{d\alpha} = 0. \tag{36}$$

This equation can be immediately integrated to give

$$\ln\frac{V}{V_0} = \frac{(1-\sin\varphi)}{\cos\varphi}(\psi - \psi_0). \tag{37}$$

Comparing (34) and (37), one can conclude that p and V satisfy (16).

Let β-lines be straight and the velocity vector be tangent to the η-lines. As in the previous case, u_α, u_β, and V are independent of β. Equations (20) and (35) are valid. Then, the first equation in (21) can be rewritten as

$$\cos\varphi\frac{dV}{d\alpha} + V(1+\sin\varphi)\frac{d\psi}{d\alpha} = 0. \tag{38}$$

Integrating this equation, one gets

$$\ln\frac{V}{V_0} = -\frac{1+\sin\varphi}{\cos\varphi}(\psi - \psi_0). \tag{39}$$

Equations (34) and (39) are compatible if (23) is satisfied.

3.1.3. Characteristic Lines of Both Families Are Straight

Assume that both families of characteristics are straight in a region. Then, ψ is constant in this region. Equations (4), (7), (12), and (20) show that p, u_α, u_β, and V are constant independently of the direction of the velocity vector. Therefore, the motion of the region is a rigid body translation.

3.2. The Double-Shearing Model

Assume that the characteristic lines of both families are curved. Let the velocity vector be tangent to the ξ-lines (Figure 1). Using (9), one can rewrite the equations in (6) as

$$\frac{\partial u_\alpha}{\partial\alpha} - u_\beta\left(1-\sin\varphi\frac{R}{S}\right) = 0,\ \frac{\partial u_\beta}{\partial\beta} + u_\alpha\left(1-\sin\varphi\frac{S}{R}\right) = 0. \tag{40}$$

Here, R is the radius of curvature of the α-lines and S is the radius of curvature of the β-lines. These quantities have been defined in [27] as

$$\frac{1}{R} = \frac{\partial\psi}{\partial s_\alpha} \text{ and } \frac{1}{S} = -\frac{\partial\psi}{\partial s_\beta}. \tag{41}$$

It has been also shown in [27] that the quantities R_0 and S_0 defined as

$$R_0 = R\exp[(\beta-\alpha)\sin\varphi] \text{ and } S_0 = S\exp[(\beta-\alpha)\sin\varphi]. \tag{42}$$

satisfy the equations:

$$\frac{\partial R_0}{\partial\beta} = S_0 \text{ and } \frac{\partial S_0}{\partial\alpha} = -R_0. \tag{43}$$

Using these equations, one can transform the equations in (40) to

$$\frac{\partial u_\alpha}{\partial \alpha} - u_\beta\left(1 - \sin\varphi\frac{R_0}{S_0}\right) = 0,\ \frac{\partial u_\beta}{\partial \beta} + u_\alpha\left(1 - \sin\varphi\frac{S_0}{R_0}\right) = 0. \tag{44}$$

Equation (12) is valid. Eliminating u_α and u_β in (44) using (12), one gets

$$\frac{\partial \ln V}{\partial \alpha} - 1 + \sin\varphi\frac{R_0}{S_0} = 0,\ \frac{\partial \ln V}{\partial \beta} + 1 - \sin\varphi\frac{S_0}{R_0} = 0. \tag{45}$$

These equations are compatible if

$$\frac{\partial^2 \ln V}{\partial \alpha \partial \beta} = \frac{\partial^2 \ln V}{\partial \beta \partial \alpha}. \tag{46}$$

It follows from (45) and (46) that ideal flows exist if

$$\frac{\partial(R_0/S_0)}{\partial \beta} = -\frac{\partial(S_0/R_0)}{\partial \alpha}. \tag{47}$$

In general, this condition is not satisfied. However, it is in particular cases, for example, if the ratio R_0/S_0 is constant. The latter condition is satisfied in the flow of plastic material through a wedge-shaped channel with no friction. Using (43), one can represent (47) as

$$\frac{\partial^2 \ln R_0}{\partial \alpha \partial \beta} = \frac{\partial^2 \ln S_0}{\partial \alpha \partial \beta}. \tag{48}$$

Let the velocity vector be tangent to the η-lines (Figure 2). Using (44) and (20), one gets

$$\frac{\partial \ln V}{\partial \alpha} + 1 - \sin\varphi\frac{R_0}{S_0} = 0,\ \frac{\partial \ln V}{\partial \beta} - 1 + \sin\varphi\frac{S_0}{R_0} = 0. \tag{49}$$

These equations are compatible if (46) is valid.

4. Dies of Minimum Length

Dies of minimum length are obtained if singular characteristic fields appear near the die's exit. A schematic diagram of such a die and the general structure of a characteristic net are shown in Figure 3. Singular points are D and D'. The α-lines in ADF are straight lines through point D. Similarly, the β-lines in $AD'F'$ are straight lines through point D'. The die's geometry is classified by the sheet's thicknesses at the exit and entry. These parameters are denoted as $2h$ and $2h_0$, respectively. The angle γ should be found from the solution. The velocity of the rigid region at the entry is V_0, and the velocity of the rigid region at the exit is V_1. Introducing a polar coordinate system (r, θ) with its origin at D is convenient for further calculations (Figure 4).

Since the α-lines coincide with the radial direction in ADF, the angle between the principal σ_1 stress σ_1 and the radial direction equals (Figure 4)

$$\psi - \theta = \frac{\pi}{4} + \frac{\varphi}{2}. \tag{50}$$

The angle between the α-and β-lines equals $\pi/2 + \varphi$. Therefore, the equation for determining curve AF is

$$\frac{dr}{rd\theta} = -\tan\varphi. \tag{51}$$

It follows from the geometry of Figure 3 that

$$\theta = -\frac{\pi}{4} - \frac{\varphi}{2} \text{ and } r = \frac{h}{\cos\left(\frac{\pi}{4} - \frac{\varphi}{2}\right)} \tag{52}$$

at A. The solution of Equation (51) satisfying the condition (52) is

$$r = \frac{h}{\cos\left(\frac{\pi}{4} - \frac{\varphi}{2}\right)} \exp\left[-\tan\varphi\left(\theta + \frac{\pi}{4} + \frac{\varphi}{2}\right)\right]. \tag{53}$$

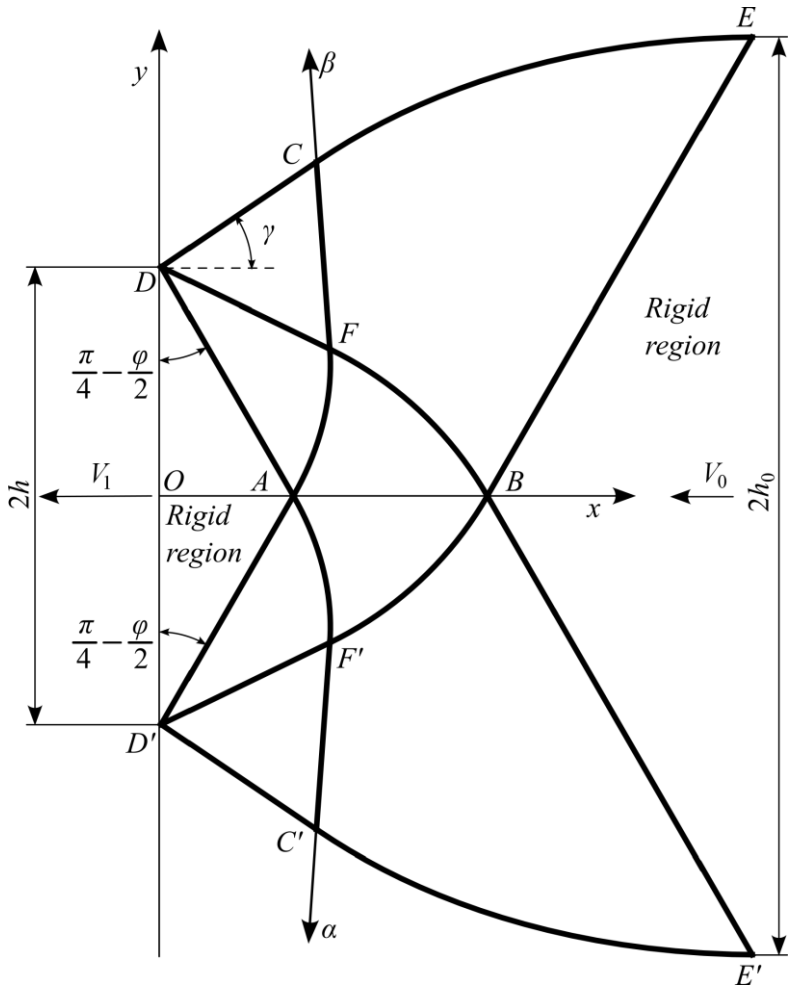

Figure 3. A schematic of the die and a characteristic net.

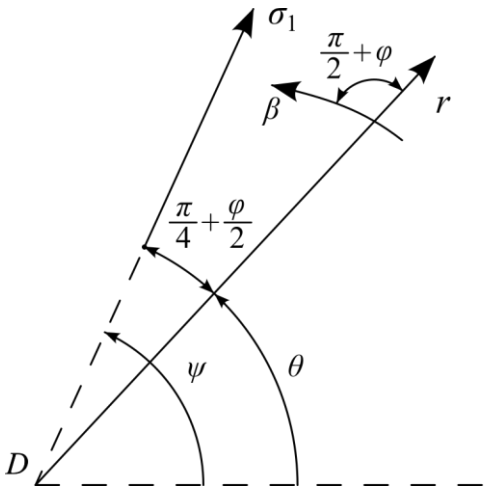

Figure 4. Characteristic lines in region ADF; r-lines coincide with α-lines.

Using this solution, one can find the radius of curvature of line AF as

$$|S| = \frac{\left(r^2 + r'^2\right)^{3/2}}{\left|r^2 + 2r'^2 - rr''\right|}, \tag{54}$$

where $r' \equiv dr/d\theta$ and $r'' \equiv d^2r/d\theta^2$. It follows from (41), (53), and (54) that

$$S = -\frac{h}{\cos\varphi \cos\left(\frac{\pi}{4} - \frac{\varphi}{2}\right)} \exp\left[-\tan\varphi\left(\theta + \frac{\pi}{4} + \frac{\varphi}{2}\right)\right]. \tag{55}$$

The origin of the characteristic coordinates can be chosen at A. Then, $\alpha = 0$ along AC and $\beta = 0$ along AC'. Using (9) and (50), one can transform (55) to

$$S = -\frac{h}{\cos\varphi \cos\left(\frac{\pi}{4} - \frac{\varphi}{2}\right)} \exp(-\beta \sin\varphi). \tag{56}$$

Comparing the second equation in (42) and (56) yields

$$S_0 = -\frac{h}{\cos\varphi \cos\left(\frac{\pi}{4} - \frac{\varphi}{2}\right)}. \tag{57}$$

on AF.

Using the line of reasoning above, it is possible to show that

$$R = -\frac{h}{\cos\varphi \cos\left(\frac{\pi}{4} - \frac{\varphi}{2}\right)} \exp(\alpha \sin\varphi) \text{ and } R_0 = -\frac{h}{\cos\varphi \cos\left(\frac{\pi}{4} - \frac{\varphi}{2}\right)}. \tag{58}$$

on AF'.

Both families of the characteristics are straight in DFC and $D'F'C'$. Therefore, DC and $D'C'$ are straight lines. Let γ be the inclination of DC to the x-axis (Figure 3). The angle between CD and FD equals $\pi/4 + \varphi/2$. Therefore,

$$\theta = \gamma - \frac{\pi}{4} - \frac{\varphi}{2}. \tag{59}$$

on DF. It follows from (50) and (59) that $\psi = \gamma$ on DF. Then, the β-coordinate of point F is determined from (9) as

$$\beta_F = \frac{\gamma}{\cos\varphi}. \tag{60}$$

The r-coordinate of point F is determined from (53) and (59) as

$$r_F = \frac{h}{\cos\left(\frac{\pi}{4} - \frac{\varphi}{2}\right)} \exp(-\gamma \tan\varphi). \tag{61}$$

Then, employing (59), one can find the x- and y-coordinates of point F as

$$x_F = \frac{h\cos\left(\gamma - \frac{\pi}{4} - \frac{\varphi}{2}\right)}{\cos\left(\frac{\pi}{4} - \frac{\varphi}{2}\right)} \exp(-\gamma \tan\varphi) \text{ and } y_F = \frac{h\sin\left(\gamma - \frac{\pi}{4} - \frac{\varphi}{2}\right)}{\cos\left(\frac{\pi}{4} - \frac{\varphi}{2}\right)} \exp(-\gamma \tan\varphi) + h. \tag{62}$$

Assuming that $ds_\beta = d\beta$ on FC, and taking into account that DF and CF are of the same length, one can find the β-coordinate at point C as $\beta_C = \beta_F + r_F$. Employing (60) and (61), one can rewrite this equation as

$$\beta_C = \frac{\gamma}{\cos\varphi} + \frac{h}{\cos\left(\frac{\pi}{4} - \frac{\varphi}{2}\right)} \exp(-\gamma \tan\varphi). \tag{63}$$

It follows from the geometry of Figure 3 that the length of CD is

$$CD = 2r_F \cos\left(\frac{\pi}{4} + \frac{\varphi}{2}\right) = \frac{2h\cos\left(\frac{\pi}{4} + \frac{\varphi}{2}\right)}{\cos\left(\frac{\pi}{4} - \frac{\varphi}{2}\right)} \exp(-\gamma \tan\varphi). \tag{64}$$

Then, the x- and y-coordinates of point C are

$$x_C = \frac{2h\cos\left(\frac{\pi}{4} + \frac{\varphi}{2}\right)}{\cos\left(\frac{\pi}{4} - \frac{\varphi}{2}\right)} \exp(-\gamma \tan\varphi)\cos\gamma,\ y_C = h + \frac{2h\cos\left(\frac{\pi}{4} + \frac{\varphi}{2}\right)}{\cos\left(\frac{\pi}{4} - \frac{\varphi}{2}\right)} \exp(-\gamma \tan\varphi)\sin\gamma. \tag{65}$$

These formulae complete construction of the characteristic field on the left to AFC. The characteristic field on the left to $A'F'C'$ can be constructed by symmetry.

Considering region $AFBF'A$, both families of characteristics are curved in this region. Equation (43) has resulted from the stress equations. Therefore, it is independent of the velocity equations. The equations in (43) are equivalent to the following telegraphy equations:

$$\frac{\partial^2 R_0}{\partial\alpha\partial\beta} + R_0 = 0 \text{ and } \frac{\partial^2 S_0}{\partial\alpha\partial\beta} + S_0 = 0. \tag{66}$$

The boundary conditions are given in (57) and (58). Each equation in (66) can be integrated by the method of Riemann [28]. Applying this method to closed curve $AP_\alpha PP_\beta$ (Figure 5), one arrives at

$$\oint_{AP_\alpha PP_\beta} \left[\left(G\frac{\partial f}{\partial\alpha} - f\frac{\partial G}{\partial\alpha}\right)d\alpha + \left(f\frac{\partial G}{\partial\beta} - G\frac{\partial f}{\partial\beta}\right)d\beta\right] = 0. \tag{67}$$

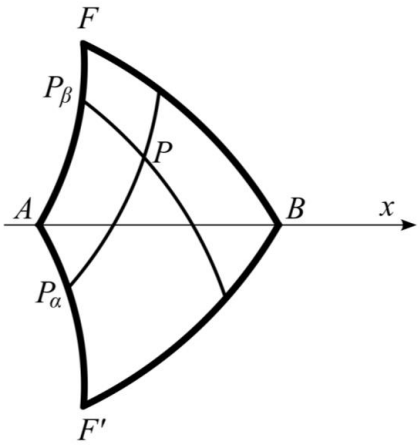

Figure 5. Characteristic lines for Riemann's method of integration ($\alpha = a$ on PP_β and $\beta = b$ on PP_α).

Here, f should be replaced with R_0 or S_0 and G is the Green's function. In the case under consideration,

$$G(a,\ b,\ \alpha,\ \beta) = J_0\left[2\sqrt{(a-\alpha)(b-\beta)}\right], \tag{68}$$

where $J_0\left[2\sqrt{(a-\alpha)(b-\beta)}\right]$ is the Bessel function of zero order. Equation (67) allows for the value of R_0 (or S_0) at point P to be calculated. In the case of the boundary value problem above, this calculation was performed in [28]. As a result,

$$\begin{aligned} R_0 &= -\frac{h}{\cos\varphi\cos\left(\frac{\pi}{4}-\frac{\varphi}{2}\right)}\left[I_0\left(2\sqrt{|\alpha\beta|}\right) + \sqrt{\left|\frac{\beta}{\alpha}\right|}I_1\left(2\sqrt{|\alpha\beta|}\right)\right], \\ S_0 &= -\frac{h}{\cos\varphi\cos\left(\frac{\pi}{4}-\frac{\varphi}{2}\right)}\left[I_0\left(2\sqrt{|\alpha\beta|}\right) + \sqrt{\left|\frac{\alpha}{\beta}\right|}I_1\left(2\sqrt{|\alpha\beta|}\right)\right]. \end{aligned} \tag{69}$$

Here, $I_0(z)$ and $I_1(z)$ are the modified Bessel functions of the first kind and the zero and first orders, respectively. Substituting (69) into (42) yields

$$\begin{aligned} R &= -\frac{h}{\cos\varphi\cos\left(\frac{\pi}{4}-\frac{\varphi}{2}\right)}\left[I_0\left(2\sqrt{|\alpha\beta|}\right)+\sqrt{\left|\frac{\beta}{\alpha}\right|}I_1\left(2\sqrt{|\alpha\beta|}\right)\right]\exp[(\alpha-\beta)\sin\varphi], \\ S &= -\frac{h}{\cos\varphi\cos\left(\frac{\pi}{4}-\frac{\varphi}{2}\right)}\left[I_0\left(2\sqrt{|\alpha\beta|}\right)+\sqrt{\left|\frac{\alpha}{\beta}\right|}I_1\left(2\sqrt{|\alpha\beta|}\right)\right]\exp[(\alpha-\beta)\sin\varphi]. \end{aligned} \tag{70}$$

Equations (9) and (41) result in

$$ds_\alpha = R\cos\varphi d\alpha \text{ and } ds_\beta = -S\cos\varphi d\beta. \tag{71}$$

It follows from this equation and the geometry of Figure 1 that

$$\begin{aligned} \tfrac{\partial x}{\partial\alpha} &= R\cos\varphi\cos\left(\psi-\tfrac{\pi}{4}-\tfrac{\varphi}{2}\right),\ \tfrac{\partial x}{\partial\beta} = S\cos\varphi\sin\left(\psi-\tfrac{\pi}{4}+\tfrac{\varphi}{2}\right), \\ \tfrac{\partial y}{\partial\alpha} &= R\cos\varphi\sin\left(\psi-\tfrac{\pi}{4}-\tfrac{\varphi}{2}\right),\ \tfrac{\partial y}{\partial\beta} = -S\cos\varphi\cos\left(\psi-\tfrac{\pi}{4}+\tfrac{\varphi}{2}\right). \end{aligned} \tag{72}$$

Using (9) and (70), one can express the right-hand sides of these equations as functions of α and β. Then, x and y can be found as functions of α and β by integration. For determining the die's shape, it is sufficient to find curves FB and $F'B$.

Considering curve FB, here, $\beta = \beta_F$ on this curve and $\alpha = 0$ at F. Point B is on the axis of symmetry. Therefore, $\psi = 0$ and, as follows from (9), $\alpha = -\beta$ at B. Using (60), one can find

$$\alpha = \alpha_B = -\gamma/\cos\varphi \tag{73}$$

at B. Curve FB is now determined from (72) as

$$x = \cos\varphi\int_0^\alpha R\cos\left(\psi-\frac{\pi}{4}-\frac{\varphi}{2}\right)d\omega + x_F,\ y = \cos\varphi\int_0^\alpha R\sin\left(\psi-\frac{\pi}{4}-\frac{\varphi}{2}\right)d\omega + y_F, \tag{74}$$

where $\beta = \gamma/\cos\varphi$ and $-\gamma/\cos\varphi \le \alpha \le 0$. Moreover, x_F and y_F are provided in Equation (63). The x-coordinate of point B is determined from (74) as

$$x_B = \cos\varphi\int_0^{-\gamma/\cos\varphi} R\cos\left(\psi-\frac{\pi}{4}-\frac{\varphi}{2}\right)d\alpha + x_F. \tag{75}$$

Curve $F'B$ is calculated similarly.

It remains to calculate the shape of CE. The β-lines are straight in region $FCEBF$. Therefore, ψ is independent of β. Its value is determined from (9) and (60) as

$$\psi = \alpha\cos\varphi + \gamma. \tag{76}$$

The equations in (72) should be replaced with

$$\begin{aligned} \tfrac{\partial x}{\partial\alpha} &= R\cos\varphi\cos\left(\psi-\tfrac{\pi}{4}-\tfrac{\varphi}{2}\right),\ \tfrac{\partial x}{\partial\beta} = -T(\alpha)\sin\left(\psi-\tfrac{\pi}{4}+\tfrac{\varphi}{2}\right), \\ \tfrac{\partial y}{\partial\alpha} &= R\cos\varphi\sin\left(\psi-\tfrac{\pi}{4}-\tfrac{\varphi}{2}\right),\ \tfrac{\partial y}{\partial\beta} = T(\alpha)\cos\left(\psi-\tfrac{\pi}{4}+\tfrac{\varphi}{2}\right). \end{aligned} \tag{77}$$

Here, $T(\alpha)$ is an arbitrary function of α. The compatibility equations are

$$\frac{\partial^2 x}{\partial\alpha\partial\beta} = \frac{\partial^2 x}{\partial\beta\partial\alpha} \text{ and } \frac{\partial^2 y}{\partial\alpha\partial\beta} = \frac{\partial^2 y}{\partial\beta\partial\alpha}. \tag{78}$$

Substituting (77) into (78) and taking into account (76), one gets

$$\begin{array}{l} \frac{\partial R}{\partial \beta}\cos\varphi\cos\left(\psi-\frac{\pi}{4}-\frac{\varphi}{2}\right)=-\frac{dT}{d\alpha}\sin\left(\psi-\frac{\pi}{4}+\frac{\varphi}{2}\right)-T\cos\left(\psi-\frac{\pi}{4}+\frac{\varphi}{2}\right)\cos\varphi, \\ \frac{\partial R}{\partial \beta}\cos\varphi\sin\left(\psi-\frac{\pi}{4}-\frac{\varphi}{2}\right)=\frac{dT}{d\alpha}\cos\left(\psi-\frac{\pi}{4}+\frac{\varphi}{2}\right)-T\sin\left(\psi-\frac{\pi}{4}+\frac{\varphi}{2}\right)\cos\varphi. \end{array} \tag{79}$$

Multiplying the first equation by $\sin(\psi-\pi/4-\varphi/2)$, the second by $-\cos(\psi-\pi/4-\varphi/2)$, and summing them gives

$$\frac{dT}{d\alpha}=T\sin\varphi. \tag{80}$$

The solution of this equation is

$$T=T_0e^{\alpha\sin\varphi}, \tag{81}$$

where T_0 is constant. The boundary condition on *CF* demands that $T = 1$ for $\alpha = 0$. Therefore, $T_0=1$ and (81) becomes

$$T=e^{\alpha\sin\varphi}. \tag{82}$$

Substituting (82) into the first equation in (79) yields $\cos\varphi\partial R/\partial\beta=-\exp(\alpha\sin\varphi)$. Integrating this equation gives

$$R=-\frac{1}{\cos\varphi}(\beta-\beta_F)+Y(\alpha), \tag{83}$$

where $Y(\alpha)$ is an arbitrary function of α. The dependence of R on α at $\beta=\beta_F$ is known from (70). Therefore,

$$Y=-\frac{h}{\cos\varphi\cos\left(\frac{\pi}{4}-\frac{\varphi}{2}\right)}\left[I_0\left(2\sqrt{|\alpha\beta_F|}\right)+\sqrt{\left|\frac{\beta_F}{\alpha}\right|}I_1\left(2\sqrt{|\alpha\beta_F|}\right)\right]\exp[(\alpha-\beta_F)\sin\varphi]. \tag{84}$$

Equations (60), (83), and (84) supply the distribution of R in *CFBEC*.

The tangent to curve *CE* is equally inclined to the α- and β-lines. Therefore, the equation of this curve is

$$ds_\alpha=ds_\beta \tag{85}$$

It follows from (77) that $ds_\alpha=R\cos\varphi d\alpha$ and $ds_\beta=Td\beta$. Substituting these equations into (85) and employing (82) and (83), one gets

$$\frac{d\beta}{d\alpha}=-(\beta-\beta_F)e^{-\alpha\sin\varphi}+Y(\alpha)e^{-\alpha\sin\varphi}\cos\varphi. \tag{86}$$

The boundary condition to this equation is

$$\beta=\beta_C \tag{87}$$

for $\alpha = 0$. The solution for (86) satisfying (87) is

$$\begin{array}{c} \beta-\beta_F=\cos\varphi\exp\left(\frac{\lambda^{\sin\varphi}-1}{\sin\varphi}\right)\int\limits_1^\lambda Y(-\ln\omega)\omega^{\sin\varphi-1}\exp\left(\frac{1-\omega^{\sin\varphi}}{\sin\varphi}\right)d\omega+ \\ +(\beta_C-\beta_F)\exp\left(\frac{\lambda^{\sin\varphi}-1}{\sin\varphi}\right), \end{array} \tag{88}$$

where $\lambda=e^{-\alpha}$. Note that

$$\lim_{\varphi\to0}\exp\left(\frac{\lambda^{\sin\varphi}-1}{\sin\varphi}\right)=\lambda \text{ and } \lim_{\varphi\to0}\exp\left(\frac{1-\omega^{\sin\varphi}}{\sin\varphi}\right)=\frac{1}{\omega}. \tag{89}$$

Equation (88) determines the shape of *CE* in the characteristic coordinates. This shape in the Cartesian coordinates can be found by integrating the following equations:

$$dx=\left(\frac{\partial x}{\partial\alpha}+\frac{\partial x}{\partial\beta}\frac{d\beta}{d\alpha}\right)d\alpha \text{ and } dy=\left(\frac{\partial y}{\partial\alpha}+\frac{\partial y}{\partial\beta}\frac{d\beta}{d\alpha}\right)d\alpha. \tag{90}$$

The partial derivatives are determined from (77), (82), and (83) as

$$\begin{array}{l} \frac{\partial x}{\partial \alpha} = (-\beta + \beta_F + Y(\alpha)\cos\varphi)\cos\left(\psi - \frac{\pi}{4} - \frac{\varphi}{2}\right), \ \frac{\partial x}{\partial \beta} = -e^{\alpha \sin\varphi}\sin\left(\psi - \frac{\pi}{4} + \frac{\varphi}{2}\right), \\ \frac{\partial y}{\partial \alpha} = (-\beta + \beta_F + Y(\alpha)\cos\varphi)\sin\left(\psi - \frac{\pi}{4} - \frac{\varphi}{2}\right), \ \frac{\partial y}{\partial \beta} = e^{\alpha \sin\varphi}\cos\left(\psi - \frac{\pi}{4} + \frac{\varphi}{2}\right). \end{array} \quad (91)$$

Substituting (86) and (91) into (90) gives

$$\begin{array}{l} \frac{dx}{d\alpha} = \sqrt{2}(\beta_F - \beta + Y(\alpha)\cos\varphi)\cos\psi\left[\cos\left(\frac{\varphi}{2}\right) - \sin\left(\frac{\varphi}{2}\right)\right], \\ \frac{dy}{d\alpha} = \sqrt{2}(\beta_F - \beta + Y(\alpha)\cos\varphi)\sin\psi\left[\cos\left(\frac{\varphi}{2}\right) - \sin\left(\frac{\varphi}{2}\right)\right]. \end{array} \quad (92)$$

It is understood here that $\beta_F - \beta$ is replaced with the right-hand side of (88) and ψ with the right-hand side of (76). Thus, the right-hand sides of the equations in (92) are known functions of α. These equations should be integrated numerically using the conditions $x = x_C$ and $y = y_C$ for $\alpha = 0$. The values of x_C and y_C are given in (65). The Cartesian coordinates of point E are determined from the solution of the equations in (92) at $\alpha = \alpha_B$. This value is provided in (73).

5. Effect of the Internal Friction Angle on the Optimal Die Shape

The optimal die shape has been calculated using the previous section's general solution. The dimensional analysis shows that the solution should depend on the reduction ratio h_0/h rather than separately on h and h_0.

Since $h_0 = y_E$ (Figure 3), then

$$h_0 = y_E = y_C + \int_0^{\alpha_B} \frac{dy}{d\alpha} d\alpha \quad (93)$$

where $dy/d\alpha$ is replaced with the right-hand side of the second equation in (92) and y_C with the right-hand side of the second equation in (65). Therefore, the right-hand side of (91) involves γ, and its solution supplies the dependence of this angle on the process and material parameters. This equation has been solved numerically. Figure 5 illustrates the dependence of γ on the reduction ratio and the angle of internal friction.

The die's length is determined as $l = x_E$ (Figure 3). Having found the value of γ, one can calculate x_E by integrating the first equation in (92) numerically. Figure 6 illustrates the dependence of the dimensionless die's length l/h_0 on the reduction ratio and the angle of internal friction.

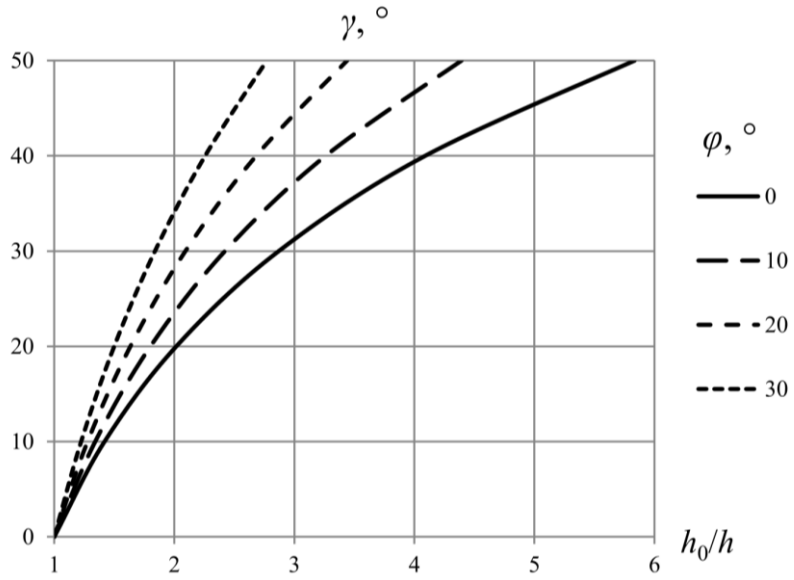

Figure 6. Dependence of the inclination angle γ on h_0/h and φ.

It is seen from Figure 6 that the inclination angle γ increases as the reduction ratio increases for a given material; the inclination angle γ increases as the angle of internal friction increases for a given reduction ratio. Figure 7 shows that the minimum die length decreases as the angle of internal

friction increases. The minimum die length may be a decreasing or non-monotonic function of the reduction ratio, depending on the angle of internal friction.

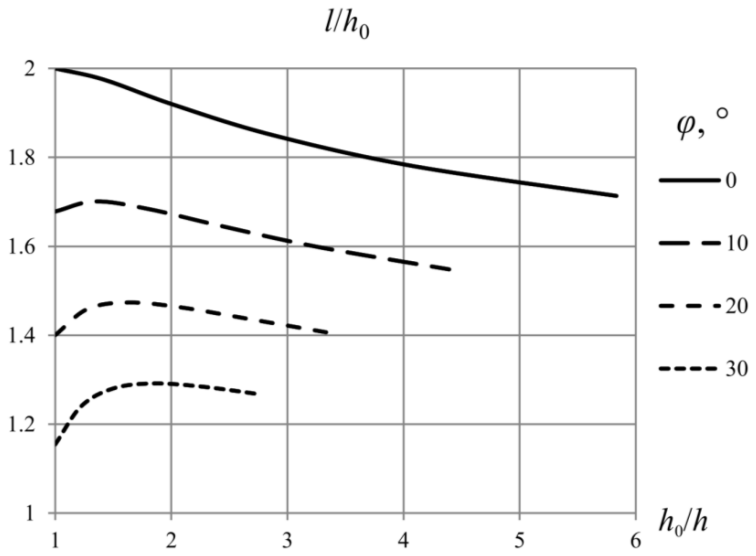

Figure 7. Dependence of the dimensionless die's length on h_0/h and φ.

The die's profile has been calculated for several values of the reduction ratio and the angle of internal friction. These profiles are depicted in Figure 8a for $h_0/h = 2$, Figure 8b for $h_0/h = 1.5$, and Figure 8c for $h_0/h = 1.2$. In all cases, the angle of internal friction is in the range $0 \leq \varphi \leq 30^0$.

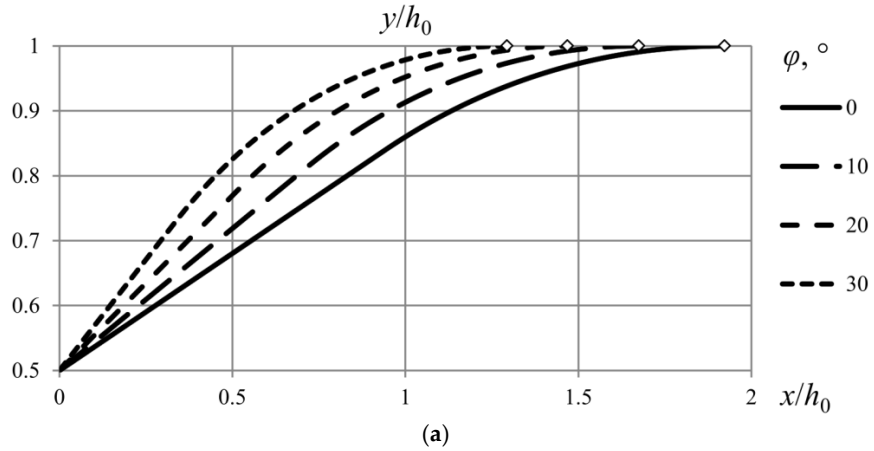

(**a**)

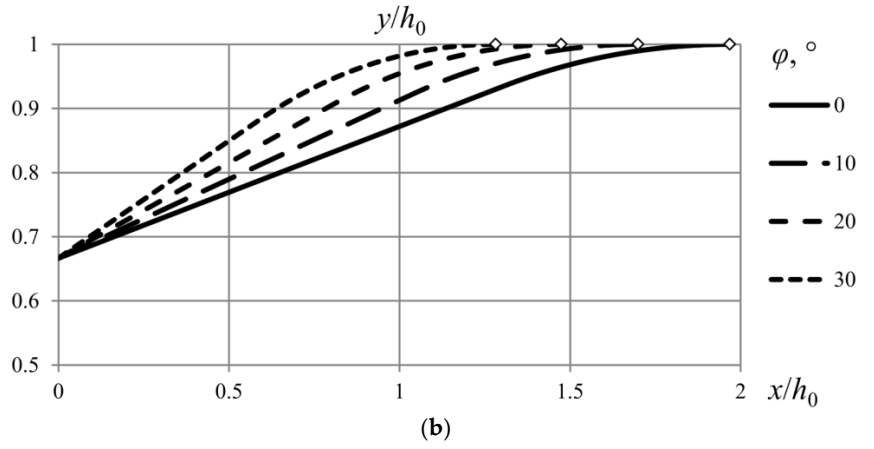

(**b**)

Figure 8. *Cont.*

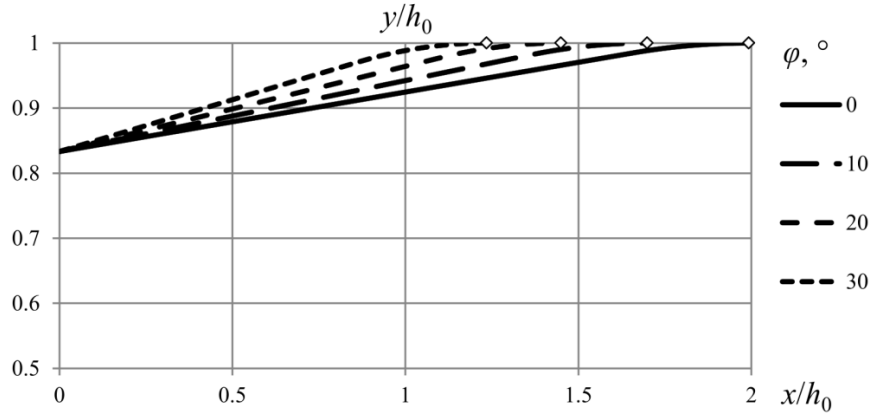

(**c**)

Figure 8. Die profiles (*DCE* curve in Figure 3) for several values of h_0/h and φ: (**a**) $h_0/h = 2$; (**b**) $h_0/h = 1.5$; (**c**) $h_0/h = 1.2$.

The stress field is important for some applications. In contrast to the die profiles above, this field depends on the process (extrusion or drawing). In particular, $\sigma_\xi = 0$ on EBE' in the case of drawing and on DAD' in the case of extrusion. The numerical results presented below are for the extrusion process. The results for the drawing process can be obtained similarly.

The distribution of pressure, $|\sigma_n|$, over the die affects its wear (see, for example, [29]). Several distributions are shown in Figure 9a for $h_0/h = 2$, Figure 9b for $h_0/h = 1.5$, and Figure 9c for $h_0/h = 1.2$. In all cases, the angle of internal friction is in the range $0 \leq \varphi \leq 30^0$. The pressure attains its maximum value at the entry point (point *E* in Figure 3), then it decreases to point *C* monotonically. The pressure is constant over the straight section of the die (*CD* in Figure 3).

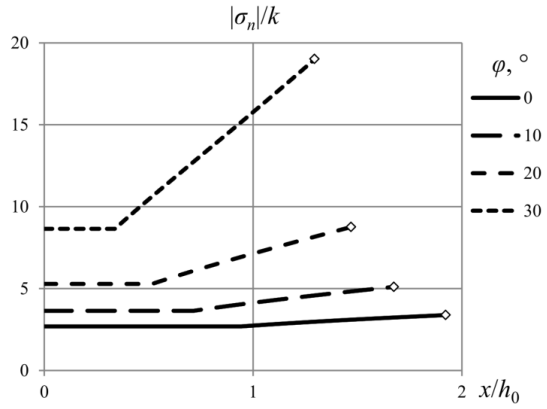

(**a**)

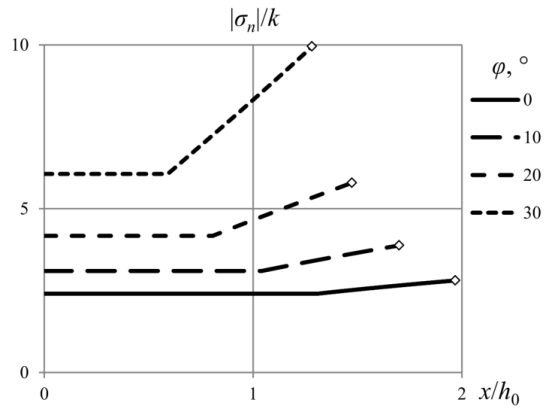

(**b**)

Figure 9. *Cont.*

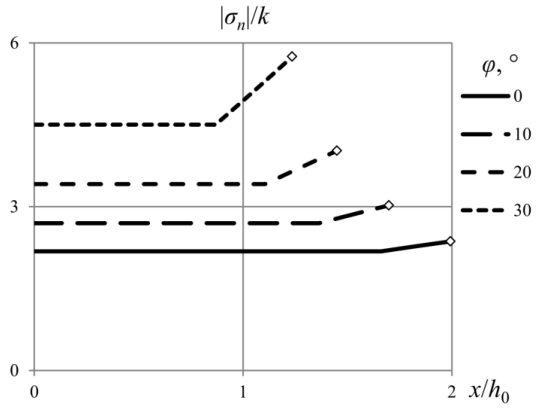

(**c**)

Figure 9. Distribution of pressure over the die for several values of h_0/h and φ: (**a**) h_0/h = 2; (**b**) h_0/h = 1.5; (**c**) h_0/h = 1.2.

The distribution of p affects ductile fracture (see, for example, [30]). A typical example is central bursting, which can appear at the symmetry axis in extrusion and drawing processes [31]. The effect of the reduction ratio and the angle of internal friction on the distribution of p along the axis of symmetry of ideal flow dies is illustrated in Figure 10 (h_0/h = 2 in Figure 10a, h_0/h = 1.5 in Figure 10b, and h_0/h = 1.2 in Figure 10c). In all cases, the angle of internal friction is in the range $0 \leq \varphi \leq 30^0$. The value of p decreases with the distance from the entry to the die independently of the process and material parameters.

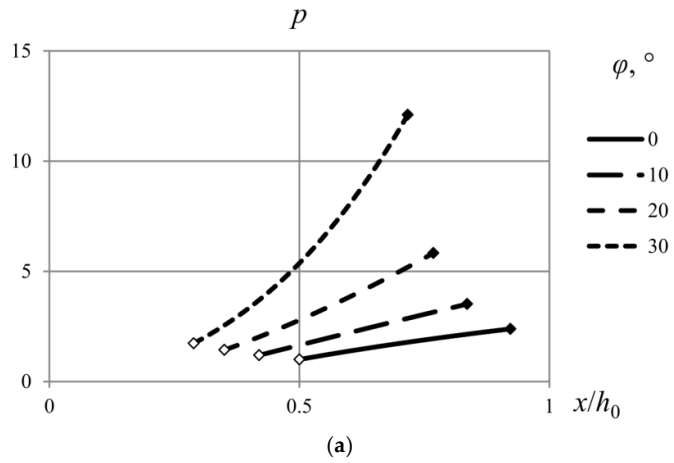

(**a**)

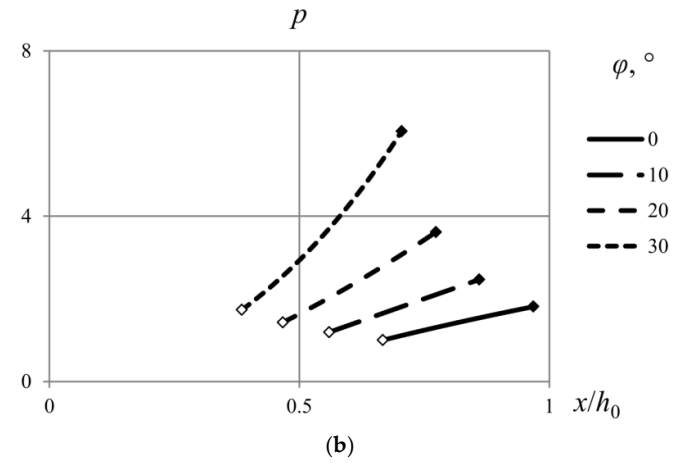

(**b**)

Figure 10. *Cont.*

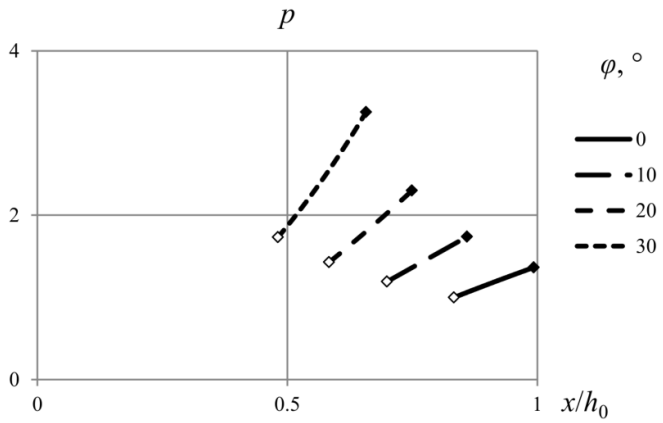

(**c**)

Figure 10. Distribution of p along the symmetry axis for several values of h_0/h and φ: (**a**) $h_0/h = 2$; (**b**) $h_0/h = 1.5$; (**c**) $h_0/h = 1.2$.

6. Conclusions

The present paper has extended the stationary bulk planar ideal plastic flow theory to the double slip and rotation model, assuming that the intrinsic spin vanishes. The new theory has been applied for calculating optimal extrusion and drawing minimum-length die profiles. It has been shown that the optimal profile depends on the angle of internal friction involved in the Mohr–Coulomb yield criterion. The double slip and rotation model reduces to the classical metal plasticity model if the angle of internal friction vanishes. The solution for the latter model has been determined as a particular case of the general solution.

The solution for the optimal dies consists of three regions. One family of characteristics is straight in the regions at the entry to and exit from the die. Moreover, the characteristic field is singular at the exit. This solution feature results from requiring the die to be of minimum length. Both families of characteristics are curvilinear in the third region. The solution for the radii of curvature of the characteristic lines in this region is written in terms of Bessel's functions. A numerical integration is required for calculating the die's profile.

Ideal flow solutions are design solutions, and they are not unique. The requirement of minimum die length allows for uniqueness to be achieved. However, other criteria can also be used. The present paper has calculated the normal pressure distribution over the die's surface. This distribution can be used in conjunction with an empirical equation for predicting the wear of the die. The distribution of the arithmetic mean of the principal stresses has been determined along the symmetry axis. This quantity is important for predicting ductile fracture. The wear of the die and ductile fracture can be used as additional design criteria.

Author Contributions: Formal analysis, V.M.; conceptualization, S.A.; supervision, S.A.; writing—original draft, S.A. and V.M. All authors have read and agreed to the published version of the manuscript.

Funding: The study was supported by the Russian State Assignment (contracts #123021700045-7, #123021700050-1).

Data Availability Statement: Not applicable.

Acknowledgments: This publication has been supported by the RUDN University Scientific Projects Grant System, project No. 202247-2-000.

Conflicts of Interest: The authors declare no conflict of interest.

References

1. Chung, K.; Alexandrov, S. Ideal Flow in Plasticity. *Appl. Mech. Rev.* **2007**, *60*, 316–335. [CrossRef]
2. Hill, R. Ideal forming operations for perfectly plastic solids. *J. Mech. Phys. Solids* **1967**, *15*, 223–227. [CrossRef]
3. Richmond, O.; Alexandrov, S. The theory of general and ideal plastic deformations of Tresca solids. *Acta Mech.* **2002**, *158*, 33–42. [CrossRef]

4. Richmond, O.; Devenpeck, M.L. A die profile for maximum efficiency in strip drawing. In Proceedings of the 4th U.S. National Congress of Applied Mechanics, New York, NY, USA, 18–21 June 1962; Rosenberg, R.M., Ed.; ASME: New York, NY, USA, 1962; pp. 1053–1057.
5. Hill, R. A remark on diagonal streaming in plane plastic strain. *J. Mech. Phys. Solids* **1966**, *14*, 245–248. [CrossRef]
6. Richmond, O.; Morrison, H.L. Streamlined wire drawing dies of minimum length. *J. Mech. Phys. Solids* **1967**, *15*, 195–203. [CrossRef]
7. Alexandrov, S.; Mustafa, Y.; Lyamina, E. Steady planar ideal flow of anisotropic materials. *Meccanica* **2016**, *51*, 2235–2241. [CrossRef]
8. Collins, I.F.; Meguid, S.A. On the Influence of Hardening and Anisotropy on the Plane-Strain Compression of Thin Metal Strip. *J. Appl. Mech.* **1977**, *44*, 271–278. [CrossRef]
9. Alexandrov, S.; Pirumov, A. A Die Profile for Maximum Efficiency in Strip Drawing of Anisotropic Materials. *Procedia Manuf.* **2018**, *21*, 60–67. [CrossRef]
10. Alexandrov, S.; Rynkovskaya, M. Review of Selected Issues in Anisotropic Plasticity under Axial Symmetry. *Symmetry* **2022**, *14*, 2172. [CrossRef]
11. Hu, L.W. Modified Tresca's yield condition and associated flow rules for anisotropic materials and applications. *J. Frankl. Inst.* **1958**, *265*, 187–204. [CrossRef]
12. Cox, A.D.; Eason, G.; Hopkins, H.G. Axially symmetric plastic deformations in soils. *Philos. Trans. R. Soc. Lond. Ser. A Math. Phys. Sci.* **1961**, *254*, 1–45. [CrossRef]
13. Coombs, W.M.; Crouch, R.S.; Heaney, C.E. Observations on Mohr-Coulomb Plasticity under Plane Strain. *J. Eng. Mech.* **2013**, *139*, 1218. [CrossRef]
14. Spitzig, W.A.; Sober, R.J.; Richmond, O. The Effect of Hydrostatic Pressure on the Deformation Behavior of Maraging and HY-80 Steels and its Implications for Plasticity Theory. *Metall. Trans. A* **1976**, *7A*, 1703–1710. [CrossRef]
15. Spitzig, W.A. Effect of hydrostatic pressure on plastic-flow properties of iron single crystals. *Acta Metall.* **1979**, *27*, 523–534. [CrossRef]
16. Lomakin, E.; Beliakova, T. Spherically symmetric deformation of solids with nonlinear stress-state-dependent properties. *Contin. Mech. Thermodyn.* **2023**. [CrossRef]
17. Cox, G.M.; Thamwattana, N.; McCue, S.W.; Hill, J.M. Coulomb–Mohr Granular Materials: Quasi-static Flows and the Highly Frictional Limit. *Appl. Mech. Rev.* **2008**, *61*, 060802. [CrossRef]
18. Ostrowska-Maciejewska, J.; Harris, D. Three-dimensional constitutive equations for rigid/perfectly plastic granular materials. *Math. Proc. Camb. Philos. Soc.* **1990**, *108*, 153–169. [CrossRef]
19. Druyanov, B. *Technological Mechanics of Porous Bodies*; Clarendon Press: New York, NY, USA, 1993.
20. Spencer, A.J.M. A theory of the kinematics of ideal soils under plane strain conditions. *J. Mech. Phys. Solids* **1964**, *12*, 337–351. [CrossRef]
21. Harris, D.; Grekova, E.F. A hyperbolic well-posed model for the flow of granular materials. *J. Eng. Math.* **2005**, *52*, 107–135. [CrossRef]
22. Alexandrov, S.; Mokryakov, V.; Date, P. Ideal Flow Theory of Pressure-Dependent Materials for Design of Metal Forming Processes. *Mater. Sci. Forum* **2018**, *920*, 193–198. [CrossRef]
23. Alexandrov, S.; Harris, D. Comparison of solution behaviour for three models of pressure-dependent plasticity: A simple analytical example. *Int. J. Mech. Sci.* **2006**, *48*, 750–762. [CrossRef]
24. Jiang, M.; Yu, H.S.; Harris, D. A novel approach to examining double-shearing type models for granular materials. *Granular Matter* **2005**, *7*, 157–168. [CrossRef]
25. Harris, D. Some Properties of a New Model for Slow Flow of Granular Materials. *Meccanica* **2006**, *41*, 351–362. [CrossRef]
26. Harris, D. Double shearing and double rotation: A generalisation of the plastic potential model in the mechanics of granular materials. *Int. J. Eng. Sci.* **2009**, *47*, 1208–1215. [CrossRef]
27. Alexandrov, S. Geometry of plane strain characteristic fields in pressure-dependent plasticity. *ZAMM-J. Appl. Math. Mech. Z. Angew. Math. Mech.* **2015**, *95*, 1296–1301. [CrossRef]
28. Hill, R. *The Mathematical Theory of Plasticity*; Oxford University Press: New York, NY, USA, 1950.
29. Farzad, H.; Ebrahimi, R. An investigation of die profile effect on die wear of plane strain extrusion using incremental slab method and finite element analysis. *Int. J. Adv. Manuf. Technol.* **2020**, *111*, 627–644. [CrossRef]
30. Gao, X.; Zhang, G.; Roe, C. A Study on the Effect of the Stress State on Ductile Fracture. *Int. J. Damage Mech.* **2010**, *19*, 75–94. [CrossRef]
31. Samy, S.N.; Saleh, C.A.R.; Ragab, A.R. Plastic flow in extrusion and drawing through conical and wedge-shaped dies: Prediction of central bursting. *Proc. Inst. Mech. Eng. Part C J. Mech. Eng. Sci.* **2006**, *220*, 1201–1210. [CrossRef]

Disclaimer/Publisher's Note: The statements, opinions and data contained in all publications are solely those of the individual author(s) and contributor(s) and not of MDPI and/or the editor(s). MDPI and/or the editor(s) disclaim responsibility for any injury to people or property resulting from any ideas, methods, instructions or products referred to in the content.